SIMULATION OF A BLIND HYPERSPECTRAL-UNMIXING ALGORITHM INCORPORATING SPATIAL CORRELATION AND SPECTRAL SIMILARITY **

Q. Li*, X. Miao

*Precision Opto-Mechatronics Technology Key Laboratory of Education Ministry,
School of Instrumentation and Optoelectronic Engineering at BeiHang University,
Beijing, 100191, China; e-mail: qbleebuaa@buaa.edu.cn, xingjin_miao@163.com*

For hyperspectral unmixing, a multi-scale spatial regularization method based on a modified image segmentation algorithm to generate super-pixels is proposed in which the super-pixels are used to extract contextual information from spatial correlations and spectral similarity in hyperspectral images (HSIs). The unmixing problem is decomposed into two simple unmixing subproblems regarding the approximate super-pixels and the original pixels. The unmixing results of these two subproblems have spatial-correlation constraints. Introducing a novel regularization term to constrain the abundance matrix to promote the homogeneous abundances helps in making effective use of the spatial correlations and spectral similarity of the abundances from HSIs. Experimental results obtained from synthetic data demonstrate that the proposed algorithm yields an accuracy greater than other conventional methods.

Keywords: *blind hyperspectral unmixing, hyperspectral image, image segmentation; multi-scale spatial regularization.*

ЧИСЛЕННЫЙ АЛГОРИТМ СЛЕПОГО ГИПЕРСПЕКТРАЛЬНОГО НЕСМЕШИВАНИЯ, СОЕДИНЯЮЩИЙ ПРОСТРАНСТВЕННУЮ КОРРЕЛЯЦИЮ И СПЕКТРАЛЬНОЕ ПОДОБИЕ

Q. Li*, X. Miao

УДК 535.317.1

*Школа приборостроения и оптоэлектронной инженерии Университета Бэйхан,
100191, Пекин, Китай; e-mail: qbleebuaa@buaa.edu.cn, xingjin_miao@163.com*

(Поступила 18 мая 2020)

Для гиперспектрального несмешивания предлагается многомасштабный метод пространственной регуляризации, основанный на модифицированном алгоритме сегментации изображения для генерации суперпикселей, в котором суперпиксели используются для извлечения контекстной информации из пространственных корреляций и спектрального сходства в гиперспектральных изображениях (HSI). Проблема разделения разложена на две простые задачи, касающиеся приблизительных суперпикселей и исходных пикселей. Результаты разделения этих задач имеют ограничения пространственной корреляции. Введение нового члена регуляризации, ограничивающего матрицу численности для обеспечения однородности численности, помогает эффективно использовать пространственные корреляции и спектральное подобие численности по данным HSI. Экспериментальные результаты, полученные на основе синтетических данных, демонстрируют более высокую точность предложенного алгоритма по сравнению с традиционными методами.

Ключевые слова: *слепое гиперспектральное несмешивание, гиперспектральное изображение, сегментация изображения, многомасштабная пространственная регуляризация.*

** Full text is published in JAS V. 88, No. 3 (http://springer.com/journal/10812) and in electronic version of ZhPS V. 88, No. 3 (http://www.elibrary.ru/title_about.asp?id=7318; sales@elibrary.ru).

Introduction. A hyperspectral image (HSI) simultaneously contains spatial and spectral information of a target that is represented by a three-dimensional data cube. For this reason, the hyperspectral imaging system is widely used for target recognition and detection by military, industrial, agricultural, and environmental agencies [1, 2]. However, because spatial resolutions of the device sensors are low, the spectral signature of each pixel in a hyperspectral image is typically “mixed” – a linearly combined spectral reflectance of the component materials. Therefore, the purpose of hyperspectral unmixing (HU) is to decompose the spectral signature of each mixed pixel into its component compositions of pure signatures from each single material, called an “endmember,” and its corresponding compositional fractions, called “abundances” [1]. At present, many different unmixing strategies have been proposed, including geometrical-based methods, dictionary-based sparse regression, and statistical-based methods.

Nonnegative matrix factorization (NMF) [3] is an ideal choice for linear unmixing because, under the assumption of no pure pixels exiting, it accomplishes synchronous estimations of the endmembers and their corresponding abundances provided with the non-negative characteristics. Unfortunately, its performance is limited by the non-convexity of the NMF objective model and noise interference. To solve these problems, some NMFs with various constraint methods have been taken into account for HU, including the minimum-distance-constrained (MDC) NMF (MDCNMF) method [4], in which differences between endmembers are controlled during the iteration. As one constraint, $L_{1/2}$-sparse regularization has been adopted in the sparsely-constrained NMF method [5]. However, these constrained NMF methods ignore rich and useful spatial-context information in HSIs, which is an important factor in reducing errors and instabilities during unmixing.

With the spatial correlations contained in HSIs, combining the useful spatial context information during the unmixing process improves the performance of HU. The total variation (TV) regularization constraint [6, 7], one of the more well-known constraints applied to HU methods incorporating spatial information, is introduced into some sparse unmixing methods to promote spatial piecewise smoothness in the abundances; however, the TV methods only consider spatial correlations between neighboring pixels while ignoring spectral similarity, which is also an important property of HSIs. In addition, the spatial neighborhood is described as a regularly shaped subregion (square window), which obviously does not conform to reality; hence, it is difficult to extract more complex spatial information from HSIs.

A new blind source unmixing method is proposed. Referred to as multi-scale spatial regularization (MSR) NMF (MSRNMF), it incorporates a spatial correlation constraint and a spectral similarity constraint. A multi-scale spatial transformation is defined that involves a modified image segmentation algorithm [8] that is used to segment HSI into a group of local spatial subregions (called super-pixels) with irregular shapes. The super-pixels are used to extract information concerning spatial correlations and spectral similarity in HSIs. The HU problem is decomposed into two subproblems to be resolved jointly over two spatial scales: one is the original scale, and the other a coarse scale constructed by super-pixels. A novel regularization term is proposed to extract both the spatial-correlation and spectral-similarity information.

Calculation. To begin giving the specific details of the proposed MSRNMF algorithm, we explain how to consider spatial priors when applying the MSR function during HU based on a linear mixing model (LMM). Next, a specific iterative optimization is described, and a specific implementation of the proposed method is presented.

Linear mixing model. The algorithm performs HU based on LMM ignoring multiple scattering [2, 3]. Specifically, with L denoting the spectral dimension and N the number of pixels, the hyperspectral LMM is described by matrix $\mathbf{P} = [p_1, p_2, \ldots, p_N] \in R^{(L\times N)}$ obtained from

$$\mathbf{P} = \mathbf{WZ} + \mathbf{E}, \tag{1}$$

where $\mathbf{W} = [w_1, w_2, \ldots, w_N] \in R^{(L\times M)}$ denotes the endmember matrix with M the number of endmembers, $\mathbf{Z} = [\zeta_1, \zeta_2, \ldots, \zeta_N] \in R^{(M\times N)}$ the abundance matrix, composed of N abundance vectors $\zeta_i = [z_{1i}, z_{2i}, \ldots, z_{Mi}]^T$ of pixel p_i, and $\mathbf{E} \in R^{(L\times N)}$ the noise matrix. The fractional abundance should meet two physical constraints: the abundance nonnegative constraint (ANC) $z_{mi} \geq 0$ ($i = 1, \ldots, N$; $m = 1, \ldots, M$) and the abundance sum-to-one constraint (ASC) $\sum_{m=1}^{M} z_{mi} = 1(i = 1, \ldots, N)$.

Multi-scale spatial regularization NMF. The proposed MSRNMF unmixing scheme has two steps. First, using a multi-scale transformation method, the original-scale image is converted into a coarse-scale image composed of super-pixels by extracting spatial-correlation and spectral-similarity information between neighboring pixels. The spectral signatures of the super-pixels are then unmixed by solving the sparse-unmixing problem. Next, a conjugate transform is applied to the estimated coarse-scale abundances to convert the unmixed results of the coarse scale back into those of the original scale using a novel norm penalty term to promote spatial correlations and spectral similarities.

Of importance is the suitable choice of the multi-scale transformation. In a physical sense, the essential purpose of this transformation is to segment the HSI adaptively and obtain super-pixels [9]. Specifically, 1) pixels that are spectrally similar and spatially adjacent are grouped (not necessarily uniformly or regularly); 2) pixels that belong to different features are separated to preserve the irregular edges and discontinuities among the subregions, and 3) the multi-scale transformation must be related to the spectral signatures.

To explore spatial correlation while considering the spectral similarity among pixels, the traditional image segmentation algorithm was adapted for the HSI in constructing the multi-scale transformation. A modified simple linear iterative clustering (SLIC) algorithm [10] (not described here) was adopted to generate super-pixels from the HSIs. The spectral reflectance of the super-pixel formed by the multi-scale transformation is then the average value of all pixel reflectance in the segmented area. The conjugate transform is used to attribute super-pixel values to all pixels located in the corresponding area.

Through this multi-scale transformation, two coarse-scale variables are obtained, namely, $\mathbf{P}_\mathrm{C}\in R^{(L\times K)}$ and $\mathbf{Z}_\mathrm{C}\in R^{(M\times K)}$,

$$\mathbf{P} \xrightarrow{\text{multi-scale transform}} \mathbf{P}_\mathrm{C},\ \mathbf{Z} \xrightarrow{\text{multi-scale transform}} \mathbf{Z}_\mathrm{C}, \tag{2}$$

which are respectively the spectral and the abundance matrices of the super-pixels; here K ($K<N$) denotes the number of super-pixels. The sparsity-constraint unmixing problem of the super-pixels in the coarse scale is expressed as

$$\min_{\mathbf{Z}_\mathrm{C}\ge 0,\mathbf{W}\ge 0} f_\mathrm{C}\left(\mathbf{W},\mathbf{Z}_\mathrm{C};\mathbf{P}_\mathrm{C}\right)=(1/2)\left\|\mathbf{P}_\mathrm{C}-\mathbf{W}\mathbf{Z}_\mathrm{C}\right\|_\mathrm{F}^2+\lambda g\left(\mathbf{Z}_\mathrm{C}\right). \tag{3}$$

Here, parameter λ controls the contribution of the sparsity function, $g(\mathbf{Z}_C)$, which is a sigmoid measurement [11] implementing the abundance sparsity constraint and defined as

$$g\left(\mathbf{Z}\right)=\frac{1}{M}\sum_{m=1}^{M}\sum_{i=1}^{N}\left(\frac{2}{1+e^{-a\mathbf{Z}_{mi}}}-1\right), \tag{4}$$

where a is a positive parameter that controls the trade-off between sparsity and uniformity. The choice $a = 20$ performs well in approximating the L_0 norm [11].

The abundance matrix $\hat{\mathbf{Z}}_\mathrm{C}$ at the coarse scale, which is further used to normalize the unmixing problem at the original scale, is obtained after solving (3). Consequently, to transform the estimated coarse-scale abundance matrix $\hat{\mathbf{Z}}_\mathrm{C}$ back to the original scale, a conjugate transformation is introduced,

$$\hat{\mathbf{Z}}_\mathrm{C} \xrightarrow{\text{conjugate transform}} \hat{\mathbf{Z}}_\mathrm{D}, \tag{5}$$

where $\hat{\mathbf{Z}}_\mathrm{D}\in R^{(M\times N)}$ represents the approximation of the original-scale abundances, which captures the spatial correlations and spectral similarity between neighboring pixels and is used as a constraint on the abundance matrix $\mathbf{Z}$. Note that this conjugate transformation is not simply an inverse operation of the multi-scale spatial transformation, i.e., $\hat{\mathbf{Z}}_\mathrm{D} \ne \mathbf{Z}$. After the above conjugate transformation, a novel MSR as well as a sparsity regularization is introduced into the NMF optimization of the original-scale image, so that pixels that belong to the same local area should have similar abundances. The objective function of the unmixing optimization problem of the original-scale image is

$$\min_{\mathbf{Z}\ge 0,\mathbf{W}\ge 0} f_\mathrm{D}\left(\mathbf{W},\mathbf{Z};\mathbf{P}\right)=\frac{1}{2}\left\|\mathbf{P}-\mathbf{W}\mathbf{Z}\right\|_\mathrm{F}^2+\frac{\gamma}{2}\left\|\left(\mathbf{Z}-\hat{\mathbf{Z}}_\mathrm{D}\right)\mathbf{Q}\right\|_\mathrm{F}^2+\mu g\left(\mathbf{Z}\right), \tag{6}$$

where γ and μ denote regularization parameters, and $\mathbf{Q} = \mathrm{diag}(q_1, \ldots, q_N)$ denotes the weight parameter matrix. Its diagonal elements represent the degree to which each original pixel contributes to spatial similarity regularization, which is measured using the reciprocal of the spectral-spatial distance D_j [10], considering spatial correlation and spectral similarity, simultaneously. Mathematically

$$\begin{gathered} D_j=\sqrt{d_\mathrm{p}^2+\left(d_\mathrm{s}/sw\right)^2 w_\mathrm{s}^{\ 2}}, \\ d_\mathrm{p}=\cos^{-1}\left(\frac{x_j^T\overline{x}}{\left\|x_j\right\|_2\left\|\overline{x}\right\|_2}\right),\quad d_\mathrm{s}=\sqrt{(m_i-m)^2+(n_i-n)^2}, \end{gathered} \tag{7}$$

where x_j denotes the spectral reflectance of the jth pixel in the subregion, $\overline{x}$ the spectral reflectance of the super-pixel in the subregion, $[m, n]^T$ the coordinates of the spatial clustering center in the subregion, and $[m_i, n_i]^T$ the coordinates of the ith pixel in the subregion. Moreover, sw is a size parameter determining the size of the subregion, and w_s the weighting parameter trading off the spectral similarity and spatial similarity, which is set to 0.3 because in practice spectral similarity is generally more important than spatial correlations. By introducing this weight parameter matrix, it is possible to avoid losing spatial details, such as target details and obvious boundaries.

Optimization algorithm. Noting the requirements of the block-coordinate-descent algorithm, and for the objective functions (3) and (6), the optimization problem consists of three subproblems, each involving the iterative updating of 1) the coarse-scale abundance $\mathbf{Z}_C$; 2) the original-scale abundance $\mathbf{Z}$; and 3) the endmember matrix $\mathbf{W}$. To guarantee elements of $\mathbf{W}$ and $\mathbf{Z}$ are within a reasonable range during the iteration, the ASC must be taken into account. In the iterative process, before the abundance matrix is updated, the endmember matrix and the two spectral matrices are augmented [5, 11]:

$$\tilde{\mathbf{P}} = \begin{bmatrix} \mathbf{P} \\ \delta \mathbf{1}_N^{\mathrm{T}} \end{bmatrix} \quad \tilde{W} = \begin{bmatrix} \mathbf{W} \\ \delta \mathbf{1}_M^{\mathrm{T}} \end{bmatrix} \quad \tilde{\mathbf{P}}_C = \begin{bmatrix} \mathbf{P}_C \\ \delta \mathbf{1}_K^{\mathrm{T}} \end{bmatrix}, \tag{8}$$

where $\mathbf{1}_N$, $\mathbf{1}_M$, and $\mathbf{1}_K$ are all-one vectors of size N, M, and K, respectively, and δ is a positive factor controlling the effect of the ASCs. In experiments, its value was set to 15.

For each subproblem, the projection gradient descent method is used to update each unknown variable to impose the ANC. An economical but effective function, max(0, x), ensures a nonnegative result by setting negative components to zero. The update rule is then expressed as

$$\mathbf{Z}_C^{(t+1)} \leftarrow \arg\min_{\mathbf{Z}_C \ge 0} f_C\left(\mathbf{W}, \mathbf{Z}_C; \mathbf{P}_C\right) = \max\left(0, \mathbf{Z}_C^{(t)} - \mu_1 \nabla_{\mathbf{Z}_C} f_C\left(\tilde{\mathbf{W}}^{(t)}, \mathbf{Z}_C^{(t)}; \tilde{\mathbf{P}}_C\right)\right), \tag{9}$$

$$\mathbf{Z}^{(t+1)} \leftarrow \arg\min_{\mathbf{Z} \ge 0} f_D\left(\mathbf{W}, \mathbf{Z}; \mathbf{P}\right) = \max\left(0, \mathbf{Z}^{(t)} - \mu_2 \nabla_{\mathbf{Z}} f_D\left(\tilde{\mathbf{W}}^{(t)}, \mathbf{Z}^{(t)}; \tilde{\mathbf{P}}\right)\right), \tag{10}$$

$$\mathbf{W}^{(t+1)} \leftarrow \arg\min_{\mathbf{W} \ge 0} f_D\left(\mathbf{W}, \mathbf{Z}; \mathbf{P}\right) = \max\left(0, \mathbf{W}^{(t)} - \mu_3 \nabla_{\mathbf{W}} f_D\left(\mathbf{W}^{(t)}, \mathbf{Z}^{(t+1)}; \mathbf{P}\right)\right), \tag{11}$$

where μ_1, μ_2, and μ_3 denote the small learning rates determined by the Armijo algorithm [20], and t denotes the tth iteration. The gradients of the corresponding variables are

$$\nabla_{\mathbf{Z}_C} f_C\left(\tilde{\mathbf{W}}, \mathbf{Z}_C; \tilde{\mathbf{P}}_C\right) = (2\lambda/M) a \exp\left(-a\mathbf{Z}_C\right) / \left(1 + \exp\left(-a\mathbf{Z}_C\right)\right)^2 + \tilde{\mathbf{W}}^{\mathrm{T}}(\tilde{\mathbf{W}}\mathbf{Z}_C - \tilde{\mathbf{P}}_C), \tag{12}$$

$$\nabla_{\mathbf{Z}} f_D(\tilde{\mathbf{W}}, \mathbf{Z}; \tilde{\mathbf{P}}) = \tilde{\mathbf{W}}^{\mathrm{T}}(\tilde{\mathbf{W}}\mathbf{Z} - \tilde{\mathbf{P}}) + \gamma(\mathbf{Z} - \hat{\mathbf{Z}}_D)\mathbf{Q} + (2\mu/M) a \exp(-a\mathbf{Z}) / (1 + \exp(-a\mathbf{Z}))^2, \tag{13}$$

$$\nabla_{\mathbf{W}} f_D\left(\mathbf{W}, \mathbf{Z}; \mathbf{P}\right) = (\mathbf{W}\mathbf{Z} - \mathbf{P})\mathbf{Z}^{\mathrm{T}}. \tag{14}$$

For optimization during MSRNMF, some specific implementation issues need to be considered. One concerns the initialization of matrices $\mathbf{W}$ and $\mathbf{Z}$. VCA [12]-FCLS [13] is used for initialization. Another concerns the exact number of endmembers, which is assumed to be already known in our experiments. The stopping rule for the iteration requires the gradient error of the function (7) to be less than 0.001 of the initial value or the number of iterations is more than 200.

The specific steps of the spectral unmixing method based on our MSRNMF approach are summarized as:

Input: $\mathbf{P} = [p_1, p_2, \ldots, p_N] \in \mathrm{R}^{(L\times N)}$, λ, γ, μ.
Multi-scale transform:
1. Generate the spectral matrix $\mathbf{P}_C$ at coarse scales using multi-scale transform.
2. Calculate the weight of each pixel $q_j = 1/D_j$ on the basis of (7), and generate weight matrix $\mathbf{Q} = \mathrm{diag}(q_1, \ldots, q_N)$.
Initialization:
Initialize the endmember matrix $\mathbf{W}$ and abundance matrix $\mathbf{Z}$ and $\mathbf{Z}_C$.
Iterate until convergence:
1. Update $\mathbf{Z}_C$ according to (9).
2. Update $\mathbf{Z}$ according to (10).
3. Update $\mathbf{W}$ according to (11).
Return: $\mathbf{W}$ and $\mathbf{Z}$.

Results and discussion. The unmixing performance of our MSRNMF and some state-of-the-art unmixing methods (VCA-FCLS, VCA-SUnSAL-TV [7], MDC-NMF [4], and $L_{1/2}$-NMF [5]) were compared and evaluated using two simulated datasets (all codes are implemented on MATLAB R2018b). To evaluate quantitatively and compare the unmixing performance, two evaluation metrics were applied, namely, spectral angular distance (SAD) and root-mean-square error (RMSE), to evaluate the accuracy of the endmember estimation and abundance inversion, respectively. Three simulated experiments using two synthetic datasets were performed to assess and compare the effects of different multi-scale transform methods, the signal-to-noise ratio (SNR) of noise, and the endmember numbers on the performance of unmixing.

To determine the best parameter settings for the MSRNMF algorithm, a grid search was performed on each dataset, and the parameter values giving the best unmixing results were selected; the values assigned were: $\lambda = \mu = 0.10$, and $\gamma = 0.05$, and the size parameter *sw* of the modified SLIC algorithm was set to 5. For the other algorithms, the parameter values were set to those given in the corresponding references. In this paper, all experimental results are from the average of 30 random tests.

Simulation experiments on synthetic data 1. Synthetic data 1 was built comprising 221 spectral channels and 100×100 pixel images. The endmembers were composed of nine spectra (EN1–EN9) randomly selected from the USGS spectral library (Fig. 1). The generation of the corresponding abundances for each endmember was the same as that described by Hendrix and colleagues [14]. Specifically, under nonnegative and additive constraints, the *k*-means algorithm and Gaussian filtering were used to generate the corresponding abundance maps. In addition, noise with different SNRs was added to the synthetic image data.

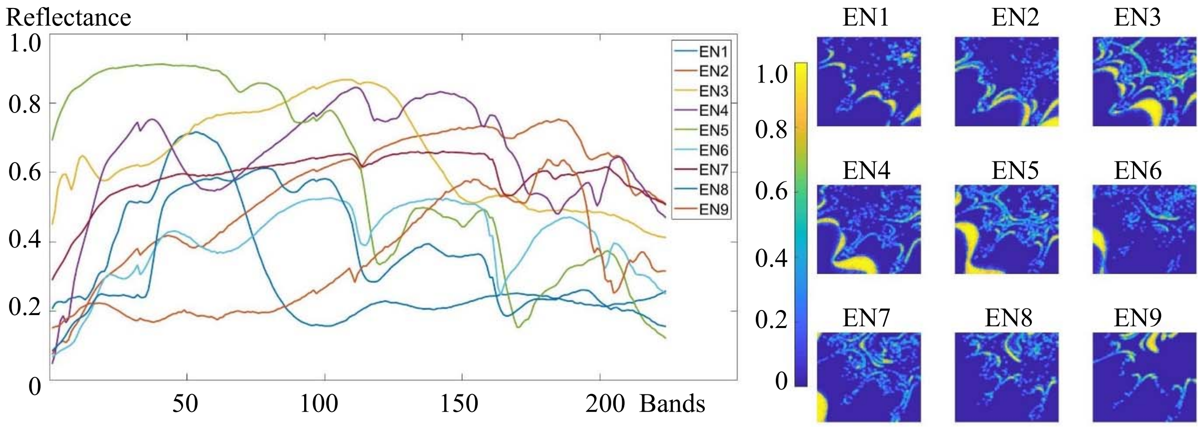

Fig. 1. Endmember spectra (EN1–EN9) and corresponding abundance images for synthetic data 1.

Simulation experiments with different multi-scale transformation methods. This experiment was designed to compare and analyze the effects of different multi-scale transformation methods on the performance of unmixing. Three different methods were selected to generate super-pixels and complete multi-scale transformation on synthetic data 1: the *k*-means method, which only considers spectral similarity; the grid method, which only considers spatial correlations; and the modified SLIC method, which considers both spectral similarity and spatial correlations. This experiment used synthetic data 1 polluted with 25 and 35 dB, Gaussian white noise. The proposed modified SLIC method was compared with the other methods in terms of the SAD and RMSE average values and corresponding standard deviations (Table 1). Clearly, our MSRNMF based on the modified SLIC method achieved a higher performance than the MSRNMF based on the *k*-means and grid methods. Because the modified SLIC method considering the spatial correlation and spectral similarity among pixels is a natural and adaptive representation of the scene, better unmixing results were obtained.

TABLE 1. MSRNMF Unmixing Performance Based on Different Multi-Scale Transformation Methods

SNR, dB	Method	SAD	RMSE
25	SLIC_HSI	0.0088(0.0009)	0.0685(0.0041)
	GRID	0.0118(0.0035)	0.0886(0.0088)
	KNN	0.0104(0.0010)	0.0711(0.0043)
35	SLIC_HSI	0.0052(0.0009)	0.0301(0.0042)
	GRID	0.0099(0.0033)	0.0474(0.0113)
	KNN	0.0075(0.0009)	0.0319(0.0049)

Robustness analysis of noise. The aim of this experiment was to compare and evaluate the noise robustness of the algorithms in application to synthetic data 1 polluted by Gaussian noise with different SNRs ranging from 20 to 45 dB in 5-dB intervals. Figure 2 shows the average SAD and RMSE values and corresponding standard deviations of different algorithms. Generally, under the same noise and SNR conditions, our MSRNMF unmixing method performed better than other unmixing methods in terms of accuracy of the endmember estimation and abundance inversion. Moreover, as SNR decreased, the average performance of all algorithms for unmixing decreased. However, because of the spatial multi-scale regularization constraints introduced, the spatial correlations and spectral similarity of the HSIs were included in the optimization system. The proposed method still performed well at low SNRs, thereby demonstrating a better robustness to noise.

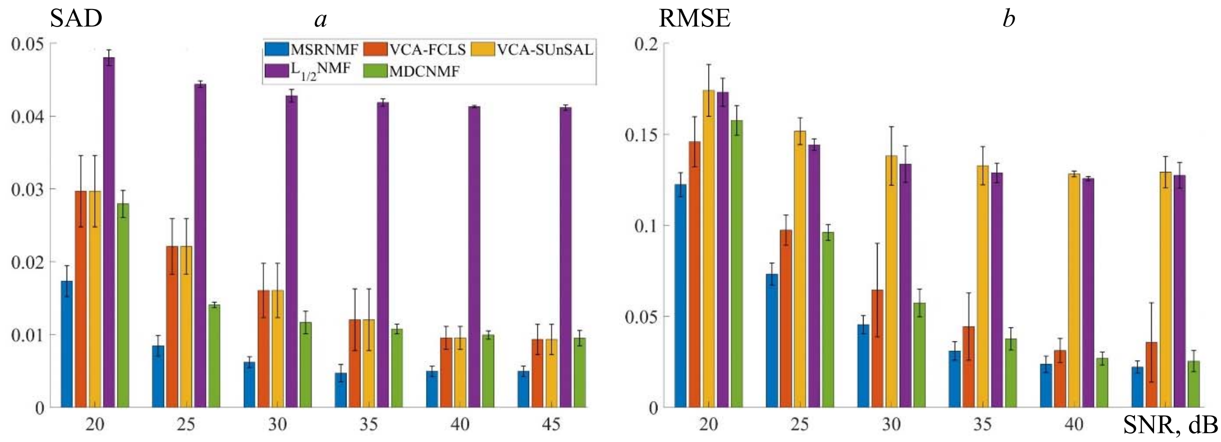

Fig. 2. Performance comparison of the algorithms at different SNR of Gaussian noise: a) SAD and b) RMSE.

Simulation experiments on synthetic data 2. Synthetic data 2, comprising 221 spectral bands and 100×100 pixel images, was generated using the MATLAB HSI synthesis simulation toolbox. To generate synthetic data 2, we randomly selected M (an odd integer from range 5–13) true endmember spectra from the USGS spectral library. The corresponding abundance maps were generated using the toolbox by selecting a spherical Gaussian field function and smoothly filtering with a nonnegative and additive constraint.

Sensitivity analysis to the number of endmembers. With the different HSIs, the number of endmembers is complex and variable, and the number of different endmembers may produce some uncertain effects when applying the algorithm. In this experiment, synthetic data 2 was used to analyze and compare the performance of each unmixing algorithm when the number of endmembers was varied from 5 to 13, and the SNR of the Gaussian white noise was fixed at 25 dB (Fig. 3). Generally, as the number of endmembers increased, the complexity of unmixing increased, whereas the accuracy of unmixing decreased. Each algorithm employed

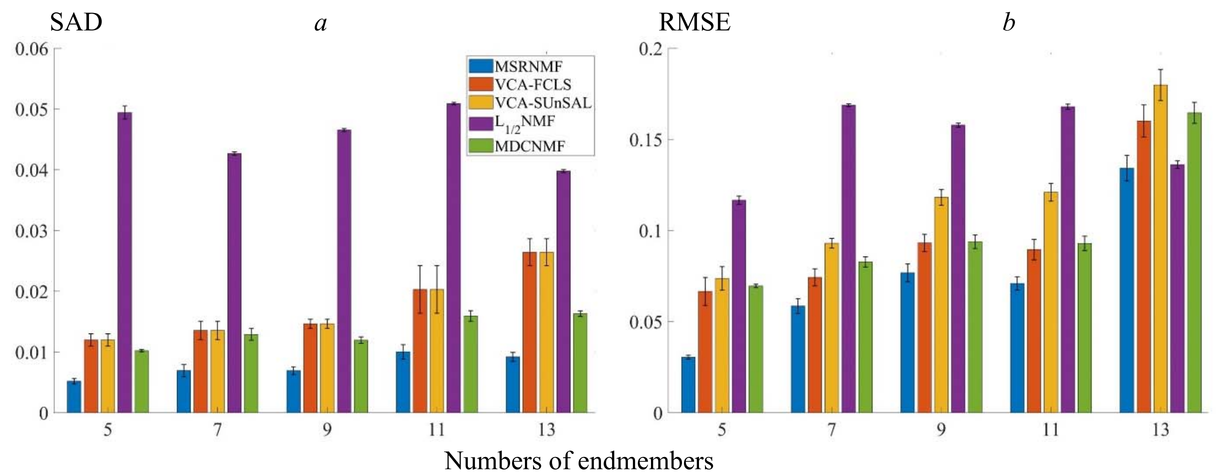

Fig. 3. Performance comparison of the algorithms with different numbers of endmembers (from 5 to 13): a) SAD and b) RMSE.

obtained better accuracy when the number of endmembers was relatively small. As the number of endmembers increased, the proposed method did not decrease the accuracy of the endmember estimation and abundance inversion, thus demonstrating its superiority. These differences were attributed to the proposed method, which contains more comprehensive constraint information, spatial multi-scale constraints, and abundance sparsity constraints.

Conclusions. A novel blind unmixing method for hyperspectral unmixing called MSRNMF was proposed. The unmixing problem was decomposed into two simples but correlated unmixing problems in the coarse-scale and original-scale image domains. Based on the modified simple linear iterative clustering image segmentation method, multi-scale spatial regularization constraint was proposed, which introduced wealth spatial priors and sparse priors as constraints during the unmixing procedure. During unmixing, the pixels in the neighborhood subspace group have a certain spatial correlation in abundance. Thus, MSRNMF captured the spatial correlation and spectral similarity in each pixel effectively. The results of the simulation experiments using synthetic data demonstrated that this method has advantages over other methods when signal-to-noise ratio is low and the number of endmembers large. Furthermore, a modified hyperspectral image segmentation algorithm was used to segment the hyperspectral image into several irregular shape subregion groups effectively, thereby providing an important improvement over traditional joint spatial information unmixing methods. Therefore, this method indicates broad potential applications in the field of hyperspectral unmixing.

This research was funded by the National Natural Science Foundation of China (grant No. 61575015).

REFERENCES

1. P. Ghamisi, N. Yokoya, L. Jun, W. Liao, S. Liu, Z. Plaza, B. Rasti, A. Plaza, *IEEE Geosci. Remote Sens. Mag.*, **5**, No. 4, 37–78 (2017).
2. Q. Li, Q. Wang, S. Shi, *J. Appl. Spectrosc.*, **86**, No. 3, 479–485 (2019).
3. H. G. Schulze, S. O. Konorov, J. M. Piret, M. W. Blades, R. F. B. Turner, *Appl. Spectrosc.*, **7**, No. 12, 2681–2691 (2017).
4. Z. Yang, G. Zhou, S. Xie, S. Ding, J. Yang, J. Zang, *IEEE Trans. Image Process.*, **20**, No. 4, 1112–1125 (2011).
5. Y. Qian, S. Jia, J. Zhou, A. Robles-Kelly, *IEEE Trans. Geosci. Remote Sens.*, **49**, No. 11, 4282–4297 (2011).
6. W. He, H. Zhang, L. Zhang, *IEEE Trans. Geosci. Remote Sens.*, **55**, No. 7, 3909–3921 (2017).
7. M.-D. Iordache, J. M. Bioucas-Dias, A. Plaza, *IEEE Trans. Geosci. Remote Sens.*, **50**, No. 11, 4484–4502 (2012).
8. R. Achanta, A. Shaji, K. Smith, A. Lucchi, P. Fua, S. Süsstrunk, *IEEE Trans. Pattern Anal. Mach. Intel.*, **34**, No. 11, 2274–2282 (2012).
9. R. A. Borsoi, T. Imbiriba, J. C. M. Bermudez, C. Richard, *IEEE Geosci. Remote Sens. Lett.*, **16**, No. 4, 598–602 (2019).
10. X. Wang, Y. Zhong, L. Zhang, Y. Xu, *IEEE Trans. Geosci. Remote Sens.*, **55**, No. 11, 6287–6304 (2017).
11. J. Li, X. Li, L. Zhao, *J. Appl. Remote Sens.*, **10**, 1–18 (2016).
12. D. C. Heinz, C.-I. Chang, *IEEE Trans. Geosci. Remote Sens.*, **39**, No. 3, 529–545 (2001).
13. J. M. P. Nascimento, J. M. Bioucas-Dias, *IEEE Trans. Geosci. Remote Sens.*, **43**, No. 4, 898–910 (2005).
14. E. M. T. Hendrix, I. Garcia, J. Plaza, G. Martin, A. Plaza, *IEEE Trans. Geosci. Remote Sens.*, **50**, No. 7, 2744–2757 (2011).